RESEARCH PAPER

Channels 8:3, 1–13; May/June 2014; © 2014 Landes Bioscience

The role of ryanodine receptor type 3 in a mouse model of Alzheimer disease

Jie Liu[1,†], Charlene Supnet[1,2,†], Suya Sun[1,†], Hua Zhang[1], Levi Good[2], Elena Popugaeva[3] and Ilya Bezprozvanny[1,3,*]

[1]Department of Physiology; University of Texas Southwestern Medical Center Dallas; Dallas, TX USA; [2]Department of Neurology and Neurotherapeutics; University of Texas Southwestern Medical Center Dallas; Dallas, TX USA; [3]Laboratory of Molecular Neurodegeneration (LMN); St.Petersburg State Polytechnical University; St. Petersburg, Russia; [†]These authors contributed equally to this work.

Keywords: ryanodine receptor, Arc, spontaneous activity, amyloid load, spine morphology, EEG, caffeine

Dysregulated endoplasmic reticulum (ER) calcium (Ca^{2+}) signaling is reported to play an important role in Alzheimer disease (AD) pathogenesis. The role of ER Ca^{2+} release channels, the ryanodine receptors (RyanRs), has been extensively studied in AD models and RyanR expression and activity are upregulated in the brains of various familial AD (FAD) models. The objective of this study was to utilize a genetic approach to evaluate the importance of RyanR type 3 (RyanR3) in the context of AD pathology.

The expression of RyanR3 was also elevated in hippocampus of APPPS1 mice (Thy1-APPKM670/671NL, Thy1-PS1L166P). In young (≤ 3 mo) APPPS1 mice, the deletion of RyanR3 increased hippocampal neuronal network excitability and accelerated AD pathology, leading to mushroom spine loss and increased amyloid accumulation. In contrast, deletion of RyanR3 in older APPPS1 mice (≥ 6 mo) rescued network excitability and mushroom spine loss, reduced amyloid plaque load and reduced spontaneous seizure occurrence.

Our data suggests a dual role for RyanR3 in AD pathology. In young AD neurons, RyanR3 protects AD neurons from synaptic and network dysfunction. In older AD neurons, increased RyanR3 activity contributes to pathology. These results imply that blockade of RyanR3 may be beneficial for those in the later stages of the disease, but RyanR activators may be beneficial when used prior to disease onset or in its initial stages. Caffeine is an activator of RyanRs and our results may help to explain a complex epidemiological connection between coffee consumption in mid-life and risk of AD development in old age.

Introduction

Accumulating evidence suggests dysregulated endoplasmic reticulum (ER) calcium (Ca^{2+}) homeostasis plays important role in synaptic loss and impaired cognitive function in Alzheimer disease (AD).[1-6] Initial data supporting the role of ER Ca^{2+} dysregulation in AD were obtained in experiments with fibroblasts isolated from pre-symptomatic patients harboring familial AD (FAD) mutations in presenilins (PSs).[7] These observations have been confirmed and extended in experiments with cells expressing mutant FAD PSs.[1-4] In addition, alterations in the expression of Ca^{2+} signaling proteins in mice and in postmortem brain samples from sporadic AD patients have been reported (see refs. 1–5 for recent reviews).

It has been demonstrated in mouse models of AD that upregulation of the ryanodine receptors (RyanRs), ER-resident Ca^{2+}-release channels, could mediate changes to intraneuronal Ca^{2+} signaling.[8] Post-mortem hippocampal brain specimens from early-stage AD patients display increased [H]^{3}ryanodine binding, indicative of increased RyanR protein levels hippocampal regions (subiculum, CA2 and CA1) compared with non-demented controls.[9] These results were recently supported in a study where post-mortem analysis of brain from individuals with mild cognitive impairment (MCI) at high risk for developing AD revealed the upregulation of RyanR type 2 (RyanR2).[10] Recent data suggest that RyanRs are increased in expression and function in FAD models, particularly in the hippocampus and cortex of PS1-M146V knock-in (KI) mice[8,11,12] and in transgenic CRND8 (APP695(KM670/671NL + V717F) mice.[13] Given the involvement of RyanRs in Ca^{2+}-induced Ca^{2+} release (CICR), modulation of membrane excitability,[14,15] neuronal function[14,16] and hippocampal learning and memory,[17,18] it is reasonable to consider that changes in RyanR expression can affect brain activity and function in AD. However, in spite of many studies focused on the role of RyanRs in AD, the data are contradictory and not conclusive. The upregulation of RyanRs may be a part of AD pathology, but it may also be a protective and/or compensatory response to neuronal Ca^{2+} dysregulation (reviewed in ref. 4). Resolving this issue is important for understanding AD pathogenesis and for validating RyanRs as potential therapeutic target for AD treatment.

*Correspondence to: Ilya Bezprozvanny; Email: ilya.bezprozvanny@utsouthwestern.edu
Submitted: 12/06/2013; Accepted: 12/09/2013; Published Online: 01/29/2014
http://dx.doi.org/10.4161/chan.27471

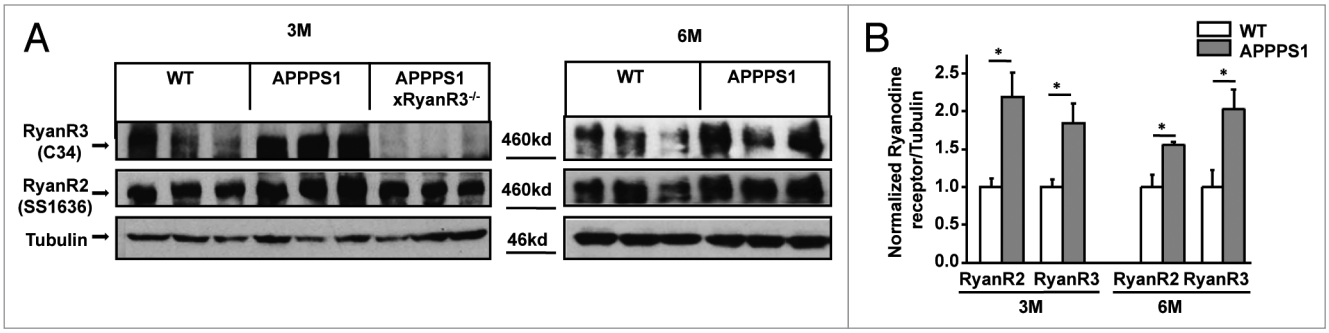

Figure 1. Expression of RyanR2 and RyanR3 is enhanced in APPPS1 hippocampal neurons. (**A**) Western blot analysis of RyanR2 and RyanR3 expression in WT and APPPS1 hippocampus at 3 and 6 mo of age. Western blot for 3 mo old APPPS1xRyanR3$^{-/-}$ also shown. Tubulin was used as a loading control. (**B**) Quantification of RyanR expression in WT and APPPS1 hippocampus. RyanR band intensity was normalized to WT and average data are shown as mean ± SE (n ≥ 3 independent experiments). On panel (**B**) the p values were calculated using a one-way ANOVA. * $P < 0.05$.

One approach used to dissect this issue is to obstruct the effects of RyanRs using pharmacological inhibitors or functional blockers. However, these approaches have yielded conflicting results.[12,13,19-22] A significant contributor to the lack of consistency across studies is the fact that pharmacological inhibitors specific to RyanR do not exist. The drug dantrolene is used in most studies to block RyanRs but it has additional targets such as store-operated Ca^{2+} channels.[23] Moreover, the 2 main RyanR subtypes expressed in the brain are RyanR type 2 (RyanR2 and RyanR type 3 (RyanR3),[24] and dantrolene has been shown to be specific to RyanR1.[25] To circumvent these pharmacology issues, we opted for a genetic approach to eliminate the contribution of RyanR. We took advantage of an RyanR3 knockout mouse (RyanR3$^{-/-}$)[26] to evaluate the importance of RyanR3 in the context of AD pathology. To achieve this goal, we selected the APPPS1 mouse (Thy1-APPKM670/671NL, Thy1-PS1L166P),[27] the same mouse model of AD that was used in our previous in vivo experiments with dantrolene.[12]

We generated APPPS1xRyanR3$^{-/-}$ mutant mice and compared them to the phenotypes of wild type (WT), RyanR3$^{-/-}$ and APPPS1 mice in young (≤ 3 mo) and old (≥ 6 mo) animals, to take into account the role of RyanR3 in AD progression and pathology. Interestingly, we discovered that RyanR3 appears to play a protective role in young mice because deletion of RyanR3 resulted in enhanced neuronal hyperexcitability and an exacerbated AD phenotype. However, deletion of RyanR3 in older mice exerted a protective effect in the context of AD pathology, resulting in normalized hyperexcitability and reduced amyloid deposition. The apparent dual role for RyanRs offers a possible explanation for the conflicting outcomes of studies that used RyanRs antagonists to treat AD mice and provide important insight as to the ideal stage in AD progression for intervention with RyanR3-targeted therapy.

Results

Expression levels of hippocampal RyanR2 and RyanR3 are increased in an AD mouse model

All 3 RyanR subtypes are expressed in the brain at the different levels of expression.[24] In previous studies we reported that RyanR expression is elevated in 3xTg (PS1-M146V KI) hippocampal neurons,[12] but the antibodies used in these studies did not discriminate between the different RyanR subtypes. Our goal was to determine if RyanRs were also elevated in expression in APPPS1 mice (Thy1-APPKM670/671NL, Thy1-PS1L166P), a model that takes into account a PS1 mutation and accumulates amyloid-β plaques in the hippocampus by 2 mo of age.[27]

To evaluate RyanR protein levels by western blot, we first had to identify subtype-specific RyanR antibodies. Our control experiments revealed that commercial antibodies used in previous studies were not specific to RyanR subtypes (data not shown). However, we were able to identify a commercially available RyanR3-specific mouse monoclonal antibody (**Fig. S1A**) and we generated RyanR2-specific rabbit polyclonal antibodies (**Fig. S1B**, see Methods for details).

To study changes in RyanR expression in APPPS1 mice over time, we performed western blots using hippocampal lysates from young (3 mo old) and older (6 mo old) WT and APPPS1 mice. It has been reported that APPPS1 mice begin to show amyloid plaque deposits in the hippocampus as early as 2 mo old and show accelerated amyloid plaque accumulation in the hippocampus between 4 and 8 mo of age.[27] We used polyclonal antibodies specific for RyanR2 (SS1636), monoclonal antibodies specific for RyanR3 (34C) (**Fig. 1**) and tubulin as the loading control in these experiments. We discovered significantly increased levels of RyanR2 and RyanR3 protein in the hippocampus of both young (3 mo old) and older (6 mo old) APPPS1 mice when compared with WT mice (**Fig. 1A and B**). From these results we concluded that RyanR2 and RyanR3 are the predominant subtypes expressed in hippocampal neurons and that expression of both RyanR2 and RyanR3 is increased approximately 2- to 3-fold in APPPS1 hippocamal neurons.

Hippocampal RyanR2 plays an essential role in brain function

Ryanodine receptor type 2 is essential for life and RyanR2 knockout is embryonic lethal in mice.[28,29] Therefore, to address the role of RyanR2 in AD we generated and validated an adeno-associated virus that expresses RNAi to knock-down RyanR2 (AAV1-RyanR2–2842) in mice (see Methods for details).

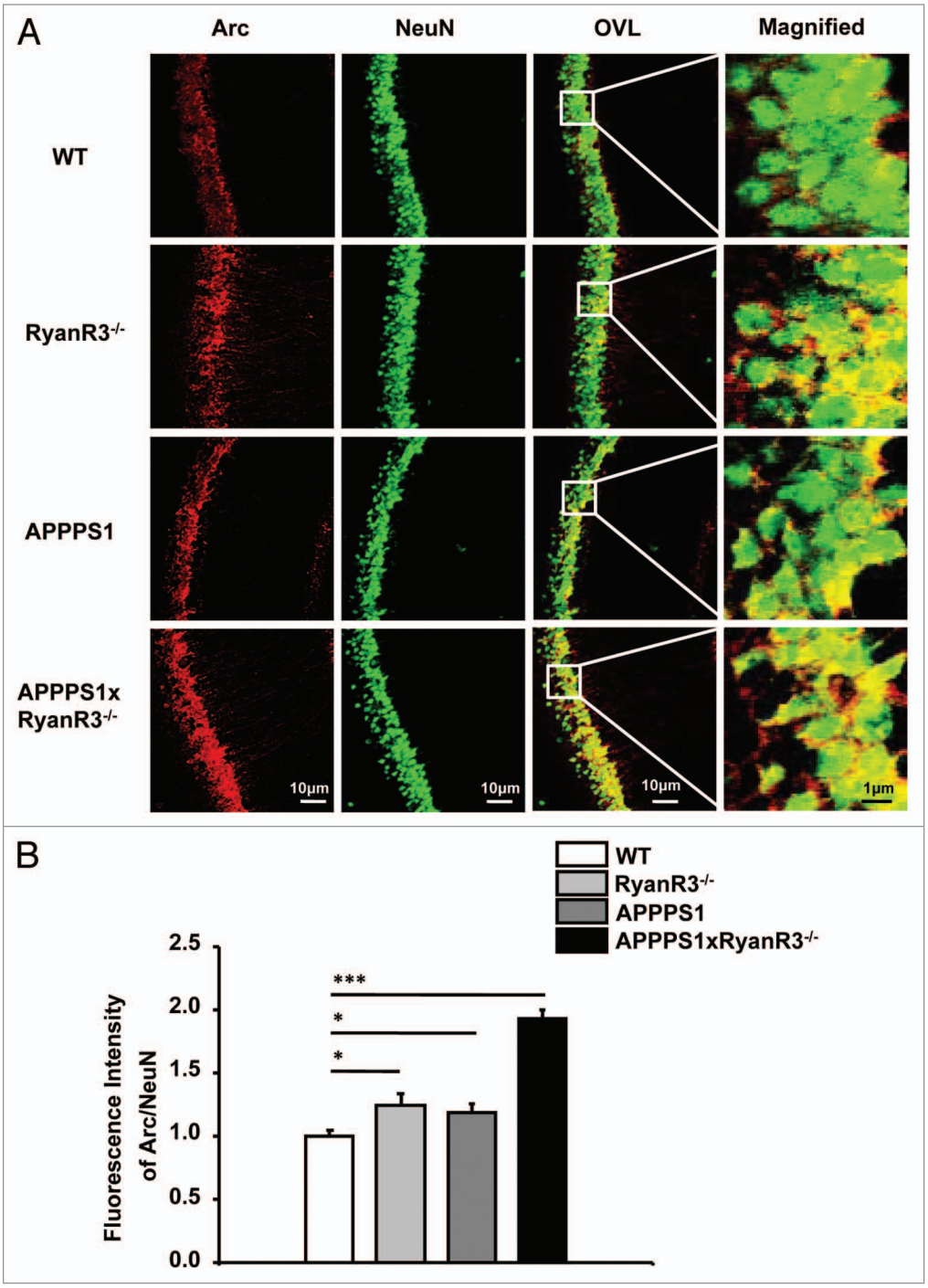

Figure 2. Arc expression is increased in APPPS1XRyanR3$^{-/-}$ hippocampus at 3 mo of age. (**A**) Representative images of CA1 regions of 3 mo old mice from different genotypes (WT, RyanR3$^{-/-}$, APPPS1, APPPS1xRyanR3$^{-/-}$) stained with Arc (red) and NeuN (green) antibodies. Overlay (yellow) is shown (OVL). The magnified region is indicated. (**B**) Quantification of the fluorescence intensity of Arc signals, which were divided by NeuN signals and normalized to WT. The average data are shown as mean ± SE (n ≥ 3 independent experiments). p values calculated using a 1-way ANOVA. *$P < 0.05$, **$P < 0.01$, ***$P < 0.001$.

Following procedures established in our laboratory,[30,31] we validated the specificity of lenti-shRNA for RyanR2 (**Fig. S1C**) and performed stereotaxic injection of AAV1-RyanR2–2842 RNAi viruses and control AAV1-NSF-GFP viruses to the hippocampal region of P0-P1 WT and APPPS1 mice. However, we discovered that within 2 mo of AAV1-RyanR2–2842 RNAi injection, WT and APPPS1 mice experienced a severe epileptic phenotype and premature death (**Fig. S2**). We terminated the study when the mice were 5 mo old due to the loss of many WT and APPPS1 mice that received the AAV1-RyanR2–2842 RNAi injection (**Fig. S2**). The morphology of hippocampal neurons in the brains of the remaining mice were analyzed

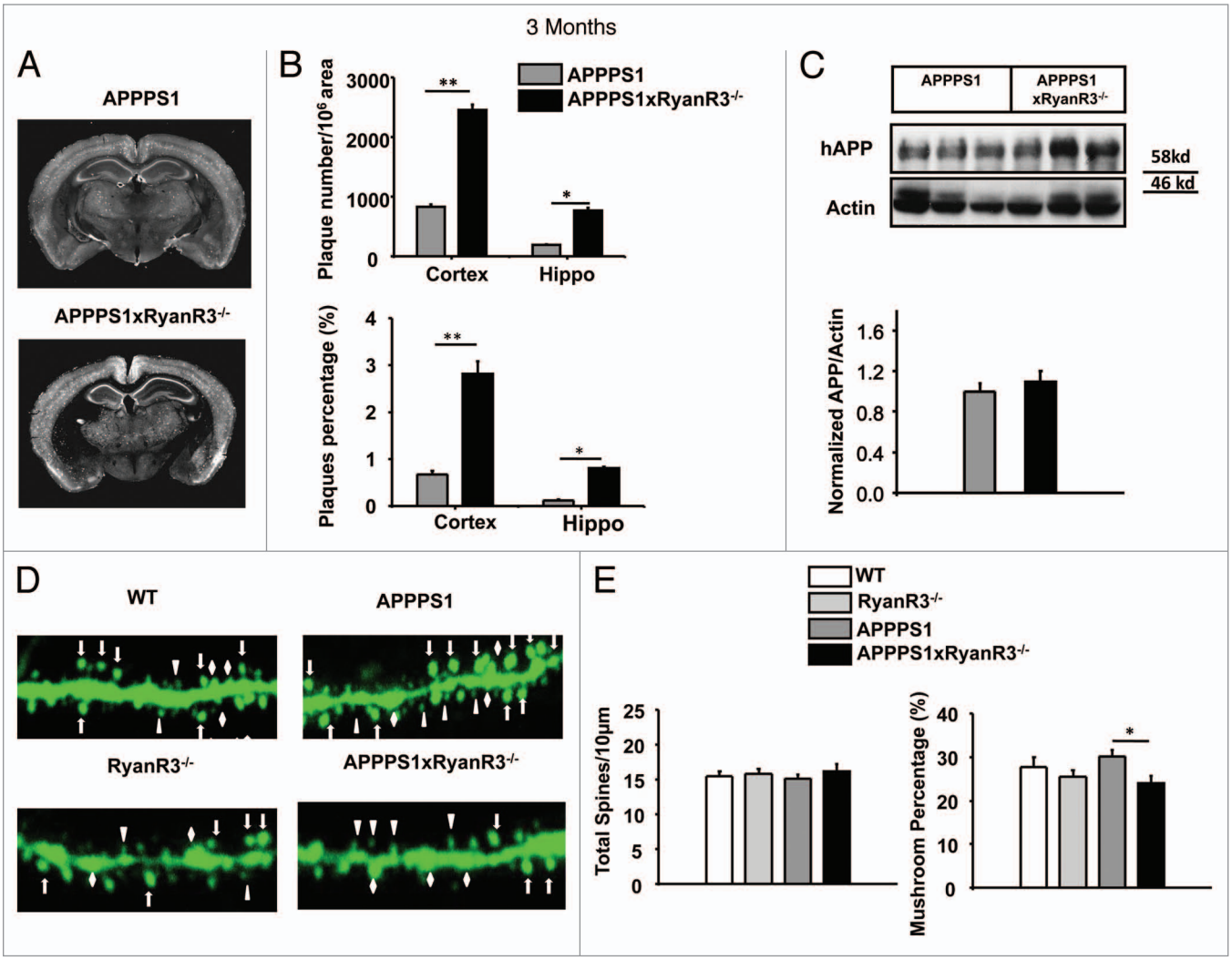

Figure 3. Deletion of RyanR3 increased amyloid load and reduced mushroom spine density in 3 mo old APPPS1 mice. (**A**) Representative coronal sections from 3 mo old APPPS1 and APPPS1xRyanR3$^{-/-}$ mice stained with 6E10 antibody (**B**) Total plaques number and the percentage of total plaques area are shown for cortical and hippocampal regions. The data are shown as mean ± SE (APPPS1, n = 6 mice; APPPS1xRyanR3$^{-/-}$, n = 5 mice). (**C**) Western blot analysis of APP levels in hippocampal lysates from 3 mo old APPPS1 and APPPS1xRyanR3$^{-/-}$. (**D**) Representative 2-photon images of spine morphology from the Lucifer yellow injected hippocampal slices of 3 mo old WT, APPPS1, RyanR3$^{-/-}$ and APPPS1xRyanR3$^{-/-}$ mice. Arrow, triangle and diamond indicate mushroom, stubby and thin spine shape, respectively. (**E**) Total spine density and fraction of mushroom spines are shown for each genotype. The data are shown as mean ± SE (WT, n = 27; RyanR3$^{-/-}$, n = 25; APPPS1, n = 33; APPPS1xRyanR3$^{-/-}$, n = 28). For the data shown on panels (**B** and **E**) *P < 0.05 and **P < 0.01 according to 1-way ANOVA analysis.

by Golgi staining. We discovered that the neuronal spine density was markedly decreased after RyanR2 knockdown for both WT and APPPS1 mice (**Fig. S3**). On average, the spine density number was 19.62 ± 0.90/10 μm in WT mice injected with AAV-GFP and 13.32 ± 0.43/10 μm in WT injected with AAV1-RyanR2–2842 RNAi virus (**Fig. S3**). For APPPS1 mice the average spine density was 15.86 ± 0.70/10 μm for the mice injected with AAV-GFP and 12.25 ± 0.70/10 μm for the mice injected with AAV1-RyR2–2842 RNAi virus (**Fig. S3**). From these results we concluded that hippocampal RyanR2 plays a major role in control of neuronal activity in the brain and is not an appropriate target for intervention due to the induction of severe epileptic phenotypes following RyanR2 knockdown in the hippocampus.

Enhanced Arc expression in hippocampus of young APPPS1xRyanR3$^{-/-}$ mice

Next, we explored the role of RyanR3 in APPPS1 mice. For these studies we took advantage of the RyanR3$^{-/-}$ mouse[26] that have a relatively mild neuronal phenotype,[17,26,32] making them appropriate for further studies. We obtained RyanR3$^{-/-}$ mice and generated APPPS1x RyanR3$^{-/-}$ mice. We confirmed the lack of RyanR3 expression in hippocampal lysates from APPPS1xRyanR3$^{-/-}$ mice (**Fig. 1A**). The levels of RyanR2 remained unchanged in hippocampus of RyanR3$^{-/-}$ mice or APPPS1x RyanR3$^{-/-}$ mice (**Fig. S1B**; **Fig. 1D**), suggesting lack of compensation by RyanR2.

What role does increased RyanR3 in the hippocampus have in AD mice? A hint lies in the physiological role of RyanR3 in

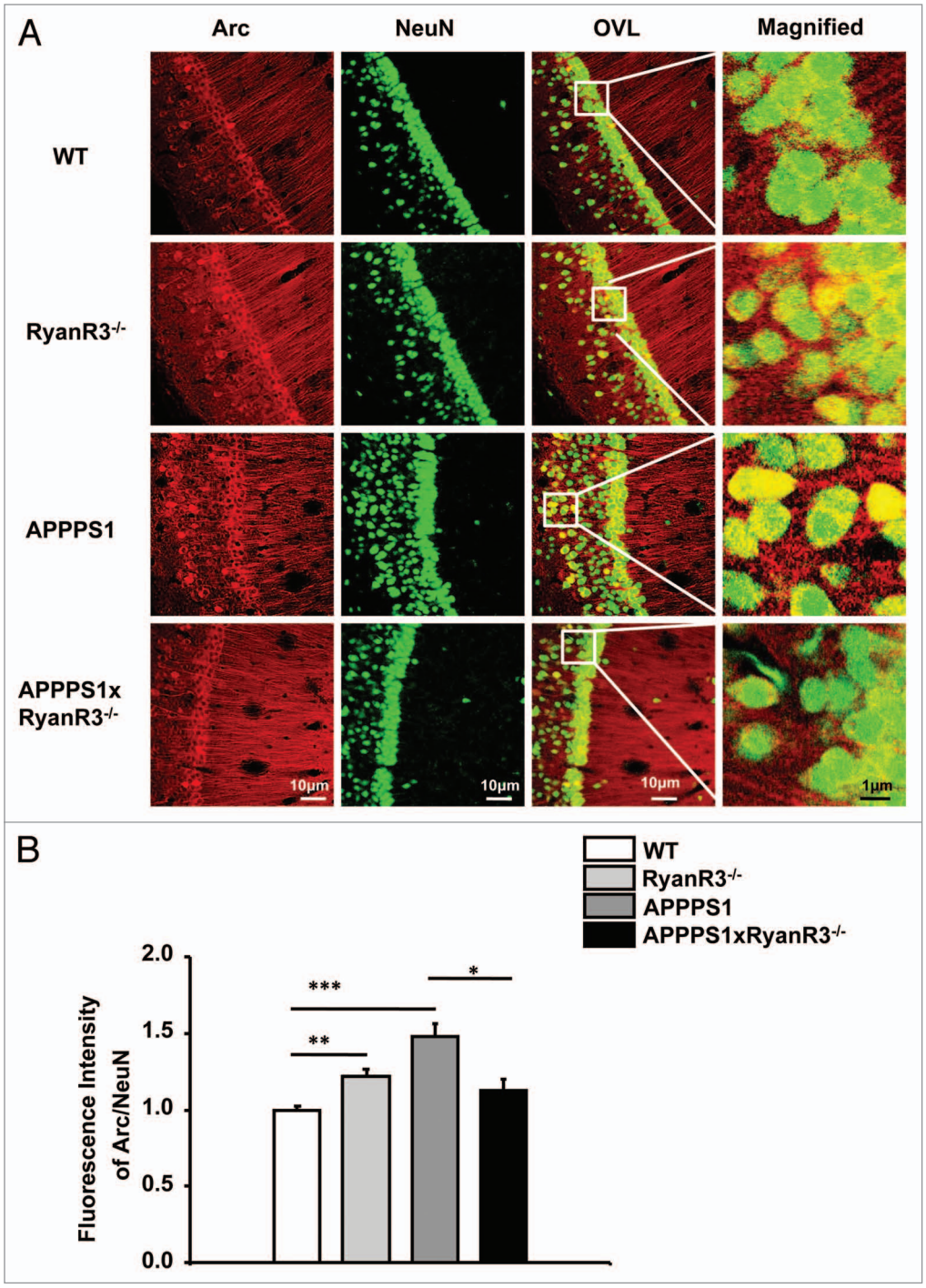

Figure 4. Arc expression is normalized in 6 mo old APPPS1XRyanR3$^{-/-}$ hippocampus.(**A**) Representative images of CA1 regions of 6 mo old mice from different genotypes (WT, RyanR3$^{-/-}$, APPPS1, APPPS1xRyanR3$^{-/-}$) stained with Arc (red) and NeuN (green) antibodies. Overlay (yellow) is shown (OVL). The magnified region is indicated. (**B**) Quantification of fluorescence intensity of Arc signals. Arc signals were divided by NeuN signals and normalized to WT. The average data are shown as mean ± SE (n ≥ 3 independent experiments). p values calculated using a one-way ANOVA. *P < 0.05, **P < 0.01, ***P < 0.001.

normal neurons. Because RyanR3 plays an important role in controlling neuronal firing rates,[14] we hypothesized that neuronal network activity could be affected in RyanR3$^{-/-}$ mice. The expression level of Arc, an immediate early gene (IEG) associated with high neuronal activity, has been used to measure neuronal excitability. The upregulation of Arc expression has been reported previously in an APP transgenic model of AD that displays neuronal network hyperexcitability.[33] We took a similar approach and evaluated Arc expression by immunostaining hippocampal slices from age-matched RyanR3$^{-/-}$, APPPS1,

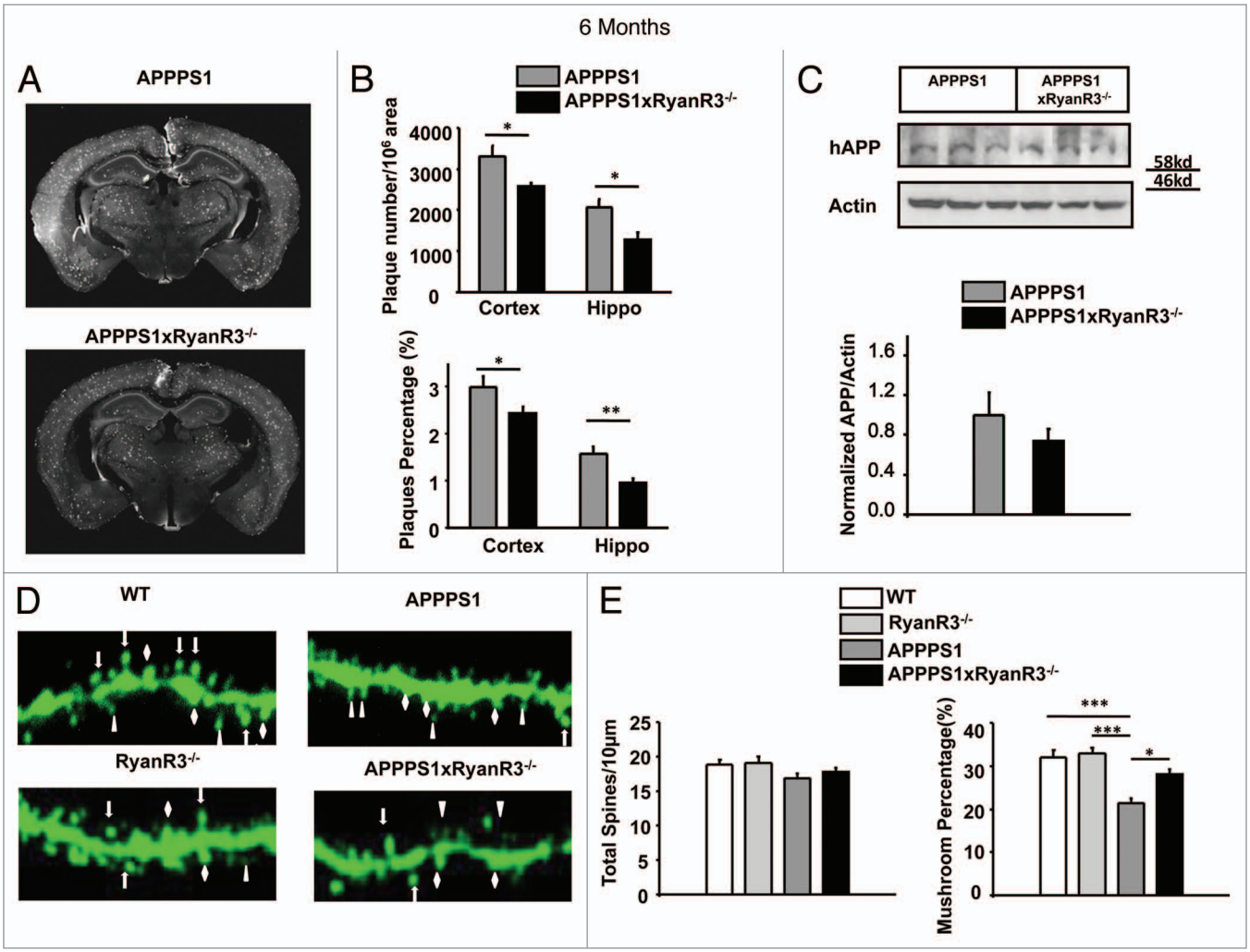

Figure 5. Deletion of RyanR3 reduced amyloid load and rescued mushroom spine loss in 6 mo old APPPS1 mice. (**A**) Representative coronal sections from 6 mo old APPPS1 and APPPS1XRyanR3$^{-/-}$ mice stained with 6E10 antibody (**B**) Total plaque number and the percentage of total plaque area are shown for cortical and hippocampal regions. The data are shown as mean ± SE (APPPS1, n = 9 mice; APPPS1xRyanR3$^{-/-}$, n = 9 mice). (**C**) Western blot analysis of APP levels in hippocampal lysates from 6 mo old APPPS1 and APPPS1xRyanR3$^{-/-}$. (**D**) Representative 2-photon images of spine morphology from the Lucifer yellow injected hippocampal slices of 6 mo old WT, APPPS1, RyanR3$^{-/-}$ and APPPS1xRyanR3$^{-/-}$ mice. Arrow, triangle and diamond indicate mushroom, stubby and thin spine shape, respectively. (**E**) Total spine density and percentage of mushroom spines are shown for each genotype. The data are shown as mean ± SE (WT, n = 24; RyanR3$^{-/-}$, n = 27; APPPS1, n = 25; APPPS1xRyanR3$^{-/-}$, n = 29). For the data shown in panels (**B**) and (**E**), $*P < 0.05$,$**P < 0.01$, $***P < 0.001$, according to 1-way ANOVA analysis.

APPPS1xRyanR3$^{-/-}$ and WT mice (**Fig. 2A**). The same slices were stained for NeuN in order to identify neuronal nuclei (**Fig. 2A**). To quantify Arc expression, the intensity of Arc staining was normalized to NeuN staining in the same slices (**Fig. 2B**). Arc levels were elevated in the hippocampus of young (3 mo old) RyanR3$^{-/-}$ mice and APPPS1 mice (**Fig. 2A and B**) compared to Arc levels in the hippocampus of WT mice, suggesting an increase in hippocampal neuronal activity in RyanR3$^{-/-}$ and APPPS1 mice. Interestingly, Arc levels were further increased in the hippocampus of young APPPS1xRyanR3$^{-/-}$ mice (**Fig. 2A and B**) compared with RyanR3$^{-/-}$ or APPPS1, suggesting a synergistic effect of RyanR3$^{-/-}$ and APPPS1 on increasing hippocampal neuronal activity. These results suggest that RyanR3 may play a role in neuronal activity and that in APPPS1 hippocampus of young (3 mo old) mice, RyanR3 is necessary to suppress neuronal activity.

Amyloid plaque accumulation is increased in young APPPS1xRyanR3$^{-/-}$ mice

The accumulation of amyloid plaques in the brain is one of the characteristic pathological markers of AD.[34,35] To determine the effect of RyanR3 deletion on plaque accumulation, we performed immunohistochemical analysis of amyloid deposits in brain slices from young (3 mo old) APPPS1 and APPPS1xRyanR3$^{-/-}$ mice. In control experiments, we confirmed no staining of amyloid observed in slices from RyanR3$^{-/-}$ and WT mice (data not shown). Coronal slices of brains from APPPS1 and APPPS1xRyanR3$^{-/-}$ mice were stained with 6E10 anti-amyloid beta (Aβ) monoclonal antibodies and imaged using a high resolution laser scanning system as we previously described.[12] Consistent with what others have reported,[27] accumulation of amyloid was observed in the hippocampal

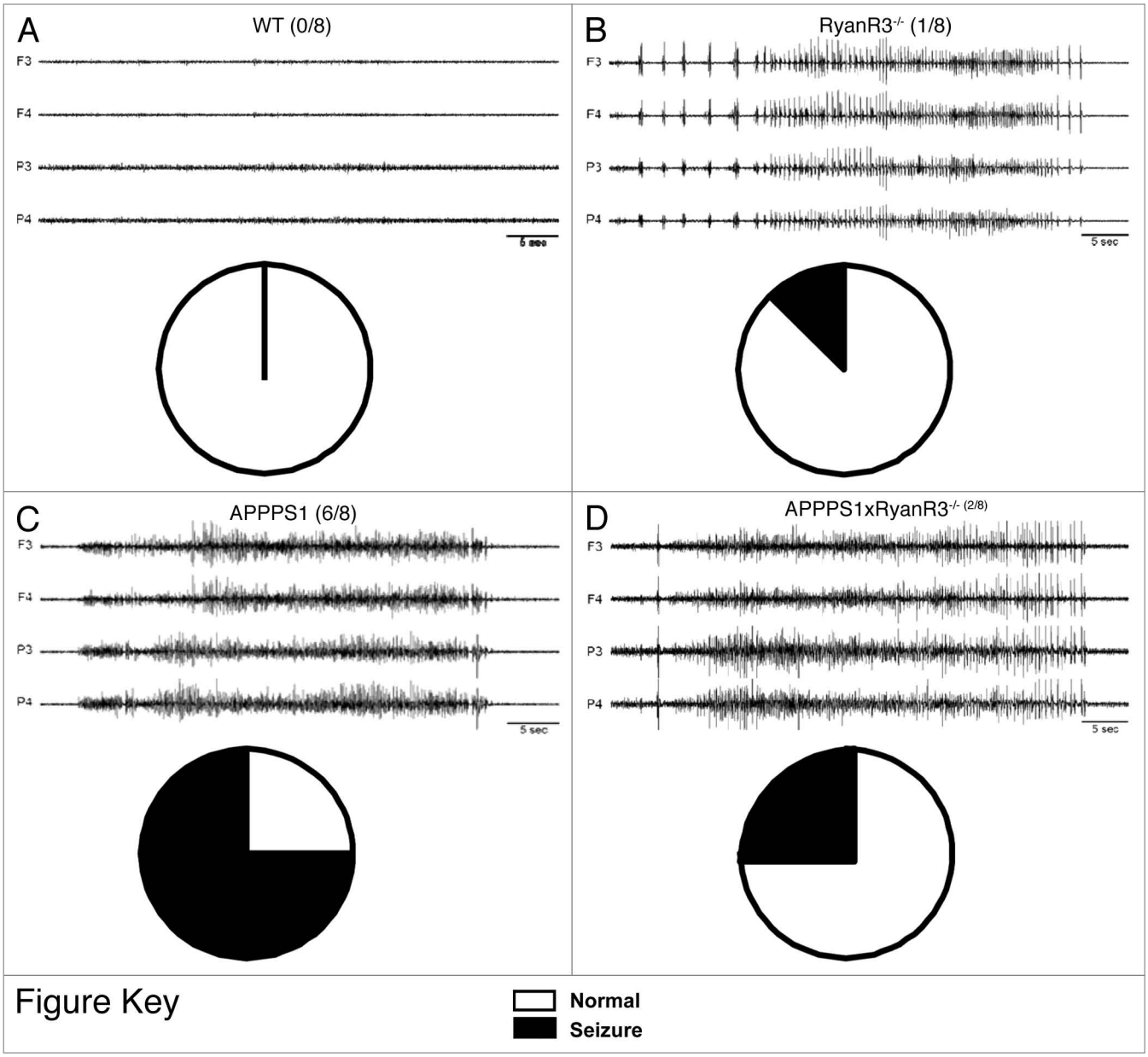

Figure 6. RyanR3 knockout rescued seizure occurrence in 11 mo old APPPS1 mice. (**A**) Example of normal EEG cortical activity is shown for WT mice. No seizures were observed in WT group (pie chart). (**B**) Example of EEG activity from RyanR3$^{-/-}$ mice. EEG shows generalized epileptic spike bursting which evolves into generalized seizure activity. Only 1 mice out of 8 (pie chart) displayed seizure activity. (**C**) Example of EEG activity from APPPS1 mice. Generalized seizure activity begins and ends abruptly. Six out of 8 mice displayed seizure activity (pie chart). (**D**). Generalized seizure activity in APPPS1 x RyanR3$^{-/-}$ mice that begins with a large epileptic spike with abrupt ending. Two out of 8 mice displayed seizure activity in this group (pie chart). EEG electrode positions for recordings shown on panels (**A–D**): F3 – left frontal, F4 – right frontal, P3 – left parietal, P4 – right parietal.

and cortical regions of APPPS1 mice at 3 mo of age (**Fig. 3A**). Amyloid plaques were more abundant and had higher signal intensity in APPPS1xRyanR3$^{-/-}$ slices when compared with APPPS1 (**Fig. 3A**). To quantify the amyloid plaques in coronal slices in APPPS1 and APPPS1xRyanR3$^{-/-}$ mice, the number of amyloid plaques (counts) and total area covered by the plaques were measured by an automated scoring algorithm (Isocyte, Molecular Devices). We found that the number of amyloid plaques and total area of plaques were significantly increased in both cortical and hippocampal regions of brains from young (3 mo old) APPPS1xRyanR3$^{-/-}$ mice when compared with their APPPS1 counterparts (**Fig. 3B**). We observed a 2- to 3-fold increase in average plaque number and a 3- to 5-fold increase in plaque area in APPPS1xRyanR3$^{-/-}$ cortex and hippocampus in these experiments (**Fig. 3B**). To determine if the increased plaque accumulation could be explained by changes in the expression of APP, we detected APP levels by western blot of hippocampal lysates from APPPS1 and APPPS1xRyanR3$^{-/-}$ mice. We found that there was no significant difference in the APP expression levels in APPPS1 and APPPS1xRyanR3$^{-/-}$ mice

(**Fig. 3C**). These findings suggest that RyanR3 may moderate amyloid accumulation in the hippocampus and cortex of young (3 mo old) APPPS1 mice.

Loss of mushroom spines in hippocampal neurons of young APPPS1xRyanR3$^{-/-}$ mice

Postsynaptic spines are classified into 3 groups according to their morphological structure. Mushroom spines have a large head and a fine neck, thin spines have a smaller head and a narrow neck, and stubby spines have no obvious distinction between the head size and the attachment to the dendritic shaft.[36,37] It has been proposed that mushroom spines are stable "memory spines" that store memories and that thin spines are "learning spines" that serve as physical substrates for the formation of new memories.[36,38] Reflecting the critical role of spines in the formation and storage of memories, significant alterations in spine number and morphology have been observed in a number of neurological and psychiatric disorders[39] and during normal aging [40]. Because memory loss is a hallmark of AD, we and others previously proposed that mushroom spines are more likely to be eliminated during AD progression.[5,6,41,42] Consistent with these predictions, it has been demonstrated that Aβ42 peptide can shift the balance from mushroom to stubby spines in the organotypic hippocampal slice culture preparation.[43]

Given the effect of RyanR3 deletion on hippocampal neuron excitability (**Fig. 2**) and amyloid production (**Fig. 3**), we hypothesized that hippocampal spine morphology could also be affected in APPPS1 neurons by deletion of RyanR3. In the next series of experiments we performed a quantitative evaluation of spine morphology in CA1 regions of pyramidal neurons from young (3 mo old) WT, RyanR3$^{-/-}$, APPPS1 and APPPS1xRyanR3$^{-/-}$ mice. These measurements were performed using 2-photon imaging of hippocampal slices that contained neurons injected with Lucifer yellow[44] (**Fig. 3D**). The shape of the spines was quantified by an automated analysis of 2-photon images using a recently published algorithm[45] (see Methods for details). After pooling data from multiple neurons and animals, we found that the total spine density was similar in hippocampus of all 4 genotypes, at the levels of 15–16 spines per 10 μm of dendrite (**Fig. 3E**). However, we found a subtle (but statistically significant) reduction in mushroom spine density in APPPS1xRyanR3$^{-/-}$ slices (23.95 ± 0.51%) compared with APPPS1 slices (30.18 ± 0.25%) (**Fig. 3E**). However, deletion of RyanR3 had no significant effect on mushroom spine density in the absence of APPPS1 mutation, nor did APPPS1 mice show increased mushroom spine density (**Fig. 3E**). These results suggest that RyanR3 may prevent subtle mushroom spine loss in young (3 mo old) APPPS1 mice. Taken together with enhanced Arc expression (**Fig. 2**) and increased amyloid accumulation (**Fig. 3**), the data suggests that RyanR3 decelerates AD pathology in young APPPS1 mice.

Reduced Arc expression in the hippocampus of older APPPS1xRyanR3$^{-/-}$ mice

The analysis of hippocampal neurons from young mice (< 3 mo) revealed that APPPS1xRyanR3$^{-/-}$ mice have enhanced expression of Arc (**Fig. 2**). Because AD is an age–related disorder, it is important to evaluate the role of RyanR3 in older or aging brains. Recently, it has been shown that aged APPPS1 mice (8 to 9 mo old) exhibit striking reductions in the number of Arc-activated cells in the dentate gyrus after a controlled spatial exploration paradigm.[46] To address the role of RyanR3 in older brains, we next focused on the analysis of Arc, neuronal excitability, amyloid plaque accumulation, mushroom spines and behavior in older (≥ 6 mo) mice of all 4 genotypes

When we evaluated Arc expression in slices from 6 mo old mice, we discovered that Arc levels were significantly elevated in RyanR3$^{-/-}$ and APPPS1 hippocampal neurons when compared with WT (**Fig. 4A and B**). These results are consistent with the Arc expression data in young mice (**Fig. 2A and B**). Paradoxically, Arc expression was not significantly elevated in APPPS1xRyanR3$^{-/-}$ hippocampal neurons when compared with WT mice and Arc levels were significantly reduced when compared with APPPS1 mice (**Fig. 4A and B**). These results suggest that deletion of RyanR3 may reduce hippocampal neuronal activity in older or aging APPPS1 hippocampal neurons, the opposite effect of RyanR3 observed in young APPPS1 hippocampal neurons (**Fig. 2A and B**).

Amyloid load is reduced in older APPPS1xRyanR3$^{-/-}$ mice

A reduction in Arc expression could indicate a decrease in hippocampal neuron activity in older (6 mo old) APPPS1xRyanR3$^{-/-}$ mice. We sought to determine the effect of RyanR3 deletion on the accumulation of amyloid plaques in older mice (6 mo old) and performed identical experiments as in young mice to quantify amyloid plaque load. Strikingly, amyloid load in the cortex and hippocampus were reduced in APPPS1xRyanR3$^{-/-}$ mice when compared with APPPS1 mice (**Fig. 5A**). Both plaque number and total surface area of the plaques were significantly lower in APPPS1xRyanR3$^{-/-}$ mice when compared with APPPS1 mice (**Fig. 5A**). These results were exactly opposite to what we observed in young (3 mo old) mice (**Fig. 3A and B**). There was a trend to reduced protein levels of hAPP in older (6 mo old) APPPS1xRyanR3$^{-/-}$ hippocampal lysates, but it was not statistically significant (**Fig. 5C**). These data suggest that RyanR3 may accelerate amyloid accumulation in older APPPS1 mice.

Deletion of RyanR3 rescues mushroom spine loss in older APPPS1 mice

As in brains from young (3 mo old) mice, we examined the effect of RyanR3 deletion in older (6 mo old) mice on the density of hippocampal neuron mushroom spines. We performed quantitative analysis of hippocampal spine morphology in 6 mo old WT, RyanR3$^{-/-}$, APPPS1, and APPPS1xRyanR3$^{-/-}$ mice using 2-photon imaging of Lucifer yellow-filled neurons (**Fig. 5D**). These experiments were performed and spine shape was quantified as described above for young brains. Our analysis revealed that the total spine density was similar for all 4 genotypes (**Fig. 5E**). There was a trend to reduced total spine density in APPPS1 mice and APPPS1xRyanR3$^{-/-}$ but it did not reach the level of statistical significance (**Fig. 5E**). However, we observed a significant reduction in the fraction of mushroom spines in APPPS1 mice compared with age-matched WT and RyanR3$^{-/-}$ mice (**Fig. 5E**). The fraction of mushroom spines in APPPS1 mice was only 21.45 ± 1.12%, significantly ($P < 0.001$)

lower than 32.04 ± 1.67% in WT mice (**Fig. 5E**). Remarkably, deletion of RyanR3 rescued the mushroom spine loss in APPPS1 mice, resulting in a mushroom spine density of 28.13 ± 1.00% in APPPS1xRyanR3$^{-/-}$ mice, which is significantly higher than in age-matched APPPS1 mice ($P < 0.05$) (**Fig. 5E**). This result is exactly opposite to what we found in young (3 mo) mice, where RyanR3 deletion exacerbated mushroom spine loss in APPPS1 mice (**Fig. 3E**). These results suggest that RyanR3 contributes to mushroom spine loss in hippocampal neurons of older APPPS1 mice. Taken together with reduced Arc expression (**Fig. 4**) and decreased amyloid accumulation (**Fig. 5A and B**), these data demonstrate that RyanR3 may exacerbate hippocampal neuron hyperactivity and AD pathology in older APPPS1 mice.

Seizure activity is reduced in older APPPS1xRyanR3$^{-/-}$ mice

We demonstrated that Arc staining intensity was decreased in hippocampal neurons of older (6 mo old) APPPS1xRyanR3$^{-/-}$ mice compared with APPPS1 (**Fig. 4**). A more direct way to measure neuronal network function is to perform electroencephalographic (EEG) recordings of electrical brain activity, a method used in previous studies to detect non-convulsive seizure activity in the hAPP-20 transgenic mouse model of AD.[33] We adapted a similar approach in our studies and performed continuous video-EEG recordings of older (11 mo old) mice during 1 wk period. For these studies we used 8 mice in each experimental group (WT, RyanR3$^{-/-}$, APPPS1, and APPPS1xRyanR3$^{-/-}$). All WT mice had no spontaneous seizures or epileptiform spikes (**Fig. 6A**). One mouse out of 8 in the RyanR3$^{-/-}$ group displayed a single seizure (35 s in duration) during the observational period (**Fig. 6B**). In contrast, 6 out of 8 mice in the APPPS1 group displayed spontaneous seizure activity (**Fig. 6C**). The frequency of seizures varied from mouse to mouse within the group, in the range of 1–8 seizures during 7 d of observation. The average seizure duration in the APPPS1 group was 32 ± 21 s (n = 27). Only 2 mice out of 8 displayed spontaneous seizure activity in APPPS1xRyanR3$^{-/-}$ group, with a single seizure for each mouse (**Fig. 6D**). The seizure durations were 40 s and 47 s for these mice. The EEG recordings of seizure activity were consistent with a generalized onset and offset, with a typical postictal depression of the EEG following offset for each group (**Fig. 6B, C, and D**). In addition, frequent generalized cortical epileptiform spikes were present in all non-WT groups including in mice where seizures were not physically evident (data not shown). These results suggest that RyanR3 may act to enhance neuronal network dysfunction and seizure activity in older APPPS1 mice.

Discussion

Enhanced expression and activity of RyanRs in familial AD models was reported by several groups,[8,10,12,13] but the significance of RyanR upregulation in AD is still unclear. In our previous studies, we suggested that augmented expression of RyanRs may be a mechanism to compensate for the loss of ER Ca^{2+} leak resulting from PS1 mutations in hippocampal neurons from PS double-knockout and PS1-M146V KI mice.[12] It has been reported that Aβ exposure can cause the upregulation of the RyanR3, but not RyanR1 or RyanR2, in cortical neurons from TgCRND8 mice, a mouse model of AD.[13] Using western blotting with subtype-specific antibodies, we detected enhanced expression of RyanR2 and RyanR3 in the hippocampus of APPPS1 mice at 3 and 6 mo of age (**Fig. 1A and B**). Does elevated expression of RyanR2 and RyanR3 play a detrimental or protective role in the context of AD pathology? It has been demonstrated that upregulation of RyanR3 may have an important role in protecting against Aβ-mediated neuronal toxicity in vitro.[19] In our previous studies, we observed that long-term feeding of the RyanR inhibitor dantrolene exacerbated amyloid plaque formation and resulted in the loss of hippocampal synaptic markers and neuronal deterioration in 8 mo old APPPS1 mice.[12] In contrast, studies from other groups showed that short-term treatment with dantrolene was able to stabilize Ca^{2+} signals, ameliorate cognitive decline and reduce neuropathology, amyloid load and memory impairments in various AD mouse models,[20-22] suggesting that blocking RyanR activity may actually be beneficial in the context of AD.

How can these seemingly divergent observations that center around the RyanRs be explained? One potential problem with interpreting these results is that specific RyanR inhibitors do not exist and the drug dantrolene, used in most studies, has additional targets such as store-operated Ca^{2+} channels.[23] Moreover, dantrolene is specific for RyanR1,[25] and does not block RyanR2 and RyanR3 effectively. To resolve this controversy, in the present study we used a genetic approach to evaluate the importance of RyanRs in the context of AD pathology in APPPS1 mice. We achieved specific knockdown of RyanR2 in hippocampus of WT and APPPS1 mice with AAV1-RyanR2–2842 RNAi (**Fig. S1**). However, we discovered that RyanR2 knockdown resulted in a severe epileptic phenotype and premature death of the infected mice (**Fig. S2**). From these results we concluded that hippocampal RyanR2 plays a major role in control of neuronal activity in the brain and is not an appropriate target for intervention due to induction of severe epileptic phenotypes following RyanR2 knockdown in hippocampus.

Next we focused on exploring the role of RyanR3 and generated APPPS1x RyanR3$^{-/-}$ mice by crossing APPPS1 with RyanR3$^{-/-}$ mouse.[26] We compared the phenotype of APPPS1x RyanR3$^{-/-}$ to the phenotype of WT, RyanR3$^{-/-}$ and APPPS1 mice. To assess the role of aging, an important aspect of AD pathology, we studied 2 cohorts of mice, young (≤ 3 mo old) and older or aging (≥ 6 mo old). These mice were within the realm of what are considered young and old APPPS1 mice with respect to AD pathology.[27,46] What we found was that RyanR3 appears to play a dual role in the context of AD pathology, rather than an invariable positive or negative effect. In the early stages of AD, it is necessary to maintain normal ER calcium homeostasis, neuronal activity/excitability, and synaptic network function. Consistent with this protective role, deletion of RyanR3 in young APPPS1 mice (≤ 3 mo old) resulted in elevated Arc expression (**Fig. 2**), increased amyloid accumulation (**Fig. 3**) and enhanced mushroom spine loss in hippocampal neurons (**Fig. 3**). The APP transgene expression in APPPS1 mice was not affected by RyanR3 deletion (**Fig. 3C**), and most likely the enhanced amyloid accumulation in APPPS1x RyanR3$^{-/-}$ mice was due to increased activity-dependent production of Aβ[47,48] as a result of

enhanced neuronal activity. These results indicate that RyanR3 plays an important protective role in early stages of AD by helping to reduce neuronal excitability and activity-dependent Aβ production. These data support the hypothesis that blockade of RyanRs in the early stages of AD progression would produce a more aggressive AD phenotype compared with the placebo group, as we previously suggested.[4,12,19] These results also suggest that pharmacological activators of RyanRs may exert beneficial effects in the early stages of AD by helping to stabilize neuronal activity. Caffeine is an activator of RyanRs and epidemiological studies have suggested that significant caffeine intake (≥ 3 cups per day) during middle-age protects from cognitive impairment and AD in old age[49-51] (but see[52]). Moreover, a recent study directly linked high blood caffeine levels to lack of progression to dementia in MCI patients.[53] It has also been demonstrated that feeding caffeine to APP transgenic mice reduces amyloid load.[54-58] It has been suggested in these studies that caffeine acts by directly suppressing the activity of β- and γ-secretases,[54-56] promoting amyloid clearance from the brain[57] or acting on adenosine receptors.[58] However, it is possible that some of the observed beneficial effects were due to the potentiating actions of caffeine on brain RyanRs, leading to reduced neuronal excitability and amyloid production.

Although RyanR3 appears to play a protective role in younger mice, our results suggest that in aging brain RyanR3 may contribute to AD pathogenesis by amplifying ER Ca^{2+} release through CICR and enhancing the dysregulation of intracellular Ca^{2+}. Indeed, in older APPPS1 mice (≥ 6 mo old) deletion of RyanR3 resulted in normalized Arc expression (**Fig. 4**), reduced amyloid load, reduced mushroom spine loss (**Fig. 5**) and reduced seizure activity (**Fig. 6**). These results consistent with reports that dantrolene exerted beneficial effects in several AD mouse models.[20-22] From this perspective it will be interesting to determine if coffee consumption by older subjects accelerates AD dementia progression.

In conclusion, we provide evidence that RyanR3 plays a dual role in the context of AD pathology. In young AD mice, RyanR3 helps to stabilize neuronal network activity and Ca^{2+} homeostasis, and genetic deletion of RyanR3 exacerbated AD phenotypes, such as amyloid accumulation and mushroom spine loss in young APPPS1 mice. In contrast, deletion of RyanR3 was beneficial to older APPPS1 mice, resulting in reduced neuronal excitability, reduced amyloid accumulation and decreased mushroom spine loss. Our study identifies RyanR3 as a potential therapeutic target for treatment of AD and also indicates that blocking RyanR3 may be beneficial in the late stages but detrimental in the early stages of the disease. Our results may also help to understand a complex epidemiological connection between coffee consumption in mid-life and the development of AD in old age.

Methods and Materials

Mice

The APPPS1 mice (Thy1-APPKM670/671NL, Thy1-PS1L166P)[27] were kindly provided by Mathias Jucker (University of Tubingen) and used in our previous studies.[12] The RyanR3$^{-/-}$ mice were previously described.[26] These mice were provided to us by Vincenzo Sorrentino (University of Siena, Italy) and Michael Mayne (University of Prince Edward Island). The colonies of all lines (on C57BL/6 background) were established at the University of Texas Southwestern Medical Center (UTSW) SPF barrier facility (vivarium). Wild-type (WT) C57BL/6 were used in experiments as control mice. All procedures involving mice were approved by the Institutional Animal Care and Use Committee of UTSW, in accordance with the National Institutes of Health Guidelines for the Care and Use of Experimental Animals.

Identification of RyanR subtype-specific antibodies

To analyze the protein levels of RyanR in hippocampal neurons we first had to identify RyanR subtype-specific antibodies. We used hippocampal tissue from WT and RyanR3$^{-/-}$ mice to test the specificity of commercially available RyanR antibodies by western blot. As a result, we identified a mouse monoclonal antibody specific for RyanR3 (clone C34, Thermo Scientific, MA3–925) (**Fig. S1A**). None of the commercial antibodies we tested were specific for RyanR2. Therefore, we generated and expressed a GST-fusion protein encoding a fragment of the mouse RyanR2 sequence 4346–4484 aa (GenBank accession number NM023868) and generated rabbit polyclonal antibodies (SS-1636) against RyanR2 as it has been previously described.[59] The specificity of generated antibody for endogenous RyanR isoforms was confirmed by western blot of brain, heart and muscle lysates (**Fig. S1B**).

Western blot analysis of hippocampal neurons and tissue

To analyze the expression of RyanR in the hippocampal regions from WT, APPPS1, RyanR3$^{-/-}$ and APPPS1XRyanR3$^{-/-}$ young (≤ 3 mo) and old (≥ 6 mo) mice, animals were anesthetized and transcardially perfused with ice-cold phosphate-buffered saline (PBS, Sigma, P4417). Brains were extracted, hippocampi dissected, and homogenized on ice. Proteins were solubilised at 4 °C for 1 h in 1% CHAPS lysis buffer on ice (1% CHAPS (Fisher Scientific (FS), BP57), 137 mM NaCl (FS, S641), 2.7 mM KCl (FS, P335), 4.3 mM Na_2HPO_4 (FS, S374), 1.4 mM KH_2PO_4 (FS, P380), pH 7.2, 5 mM EDTA (FS, BP2482), 5 mM EGTA (FS, O2783), and protease inhibitors (Roche, 04693116001). Total protein was separated by SDS-PAGE and analyzed by western blotting with anti-Ryan3 (1:500), anti-Ryan2 (1:1000), anti-APP (1:200, clone 2.F2.19B4, Millipore, MAB343), anti-tubulin (1:1000, DSHB, E7-c) and anti-actin (1:1000, clone BA3R, Thermo Scientific, MA5–15739). Horseradish peroxidise-conjugated anti-rabbit and anti-mouse secondary antibodies (115–035–146 and 111–035–144) were from Jackson ImmunoResearch. The mean density of each band was normalized to the tubulin signal in the same sample and shown as an average of at least 3 separate experiments.

Generation and validation of AAV1-RyanR2–2842 RNAi

Lenti-Ryanodine 2(RyanR 2)-shRNAi(2842 RNAi) plasmid was purchased from Sigma (TRN0000102842). RyanR2–2842 RNAi was cut and cloned into adeno-associated virus (AAV)-CMV-hrGFP plasmid behind the U6 promoter. The AAV-RyanR2–2842 RNAi plasmids were sent to the University of Iowa Gene Transfer Vector Core where serotype

1 adenoassociated viruses (AAV1s) were made using the Sf9 cell-based AAV production system. The titer of purified AAV1-RyanR2–2842 RNAi viruses provided by the University of Iowa Gene Transfer Vector Core was ≥ 1013 infectious particles/ml. In addition, control AAV1-NLS-GFP virus of similar titer was also provided by the University of Iowa Gene Transfer Vector Core. The stereotaxic injection of AAV1-RyanR2–2842 RNAi and AAV1-NLS-GFP viruses was performed on 2 mo old mice, as we described previously.[30,31] For injection of AAV1 into the hippocampus, the injection syringes were positioned on the left and right sides of the head and the optimal injection coordinates (from bregma) were anterior/posterior (AP) -2.0 mm, lateral +2.6 mm, dorsal/ventral-1.9 mm. One (1) µl total volume of virus was injected into each side. Correct targeting of the hippocampus was confirmed by GFP imaging of brain slices from the subset of the injected mice.

Golgi staining

After transcaridally perfusing with PBS, whole fresh brain was incubated in Golgi stain solution (5% potassium dichromate and 5% mercuric chloride (sublimate) mixture slowly poured into 2% potassium chromate solution [1:1]) for 14 d in the dark. After incubation, brain sections (100 µm) were obtained using a vibratome (Leica VT1200S, Leica Biosystems) and immediately mounted on Superfrost Plus glass slides (FS, 12–500). The sections were dried at 55 °C for 20–30 min, rinsed with distilled water and then incubated in 20% ammomium hydroxide (Sigma, 320145) for 20 min. Slides were rinsed twice with distilled water and fixed in Kodak fixer solution (1:7, Sigma, P6557) for 10 min. Slides were rinsed in water, dehydrated, and mounted. Pictures of Golgi stained neurons were taken using a Nikon Eclipse 80i microscope (Melville).

Immunohistochemistry

After transcardially perfusing mice with PBS followed by ice-cold 4% paraformaldehyde (PFA, FS, AC41678), brains were extracted, frozen on dry ice, and sectioned at 30 µm thickness using a Leica SM2000R microtome (Leica Biosystems). Coronal sections from the mice were stained with anti-Arc (1:100, Synaptic Systems, 156003) and anti-NeuN (1:1000, Millipore, MAB377). Images were acquired using a Zeiss LSM 510 Meta confocal microscope (Carl Zeiss Microscopy, LLC). The signal intensity of Arc was normalized to NeuN (Arc/NeuN) and was quantified from 6 regions of interest (ROIs) per slice. The average normalized signal intensity of Arc was considered the expression level of Arc.

Amyloid load was quantified as previously described for APPPS1 mice.[12] Briefly, APPPS1xRyanR3$^{-/-}$ and age-matched WT, APPPS1 and RyanR3$^{-/-}$ mice were fixed with 4% PFA. For Aβ staining, 30 µM brain slices were incubated with Beta Amyloid, 1–16 (6E10) Monoclonal Antibody (1:1000, Covance, Inc., SIG-39300–200) and Alexa488-conjugated IgG (1:500, Jackson Immunoresearch, 016–540–084) and scanned with the Isocyte Laser Scanning Imager (Molecular Devices) for quantification of amyloid load. Plaque counts and total area of plaques are used as the parameters for quantifying amyloid load.

Dendritic spine morphology in mouse hippocampus

Analysis of dendritic spine morphology was performed according to the published methods.[44] Briefly, mice of different ages and genotypes (as indicated in the text) were transcardially perfused with 45 mL of ice cold 1.5% paraformaldehyde (PFA) solution in PBS (pH7.4) for 3 min. The brains were extracted and post-fixed in 1.5% PFA solutions overnight before cutting. Thick (250–300 µm) hippocampal sections from the fixed brains were obtained using a vibratome (Leica VT1200S) and floated in 0.5% NaN_3 (FS, S2271) PBS solution at 4 °C. Sections were placed in a slice recording chamber and were viewed using an Olympus BX51 microscope (Olympus) with infrared camera portal. The glass electrodes for dye injection were prepared by the puller (Sutter Instruments, P97). The resistance of the electrodes ranged between 150–300 MΩ when filled with PBS. Hippocampal neurons in CA1 were selected visually under the microscope and patched with the electrodes filled with Lucifer yellow solution (Invitrogen, L-12926). A small constant negative current was used to monitor the dye injection (Multiclamp 700B, Molecular Devices). Successful impalement was judged by rapid and intensive dye filling of the neuron. Dye injection was facilitated by application of a constant negative current in the range of 1–3 nA for 5–15 min. Dye filling procedure was completed when very bright spines were visible. Ten to 20 neurons were injected in each section. Injected sections were analyzed by 2-photon imaging (Zeiss LSM780, Carl Zeiss Microscopy, LLC) with 40x lens and 5x zoom. The Z interval was 0.5 µm. The secondary apical dendrites of hippocampal CA1 pyramidal neurons were selected for taking images. Each image maximal resolution was 1024 × 1024 pixels and averaged 2 times. Approximately 20–30 neurons from 3–4 mice were analyzed for each genotype and age sample. To classify the shape of neuronal spines in slices we also used NeuronStudio software package and an algorithm[45] with the following cut-off values: $AR\_thin_{(crit)}$ = 2.5, $HNR_{(crit)}$ = 1.3, HD (crit) = 0.15 µm.

Electroencephalographic (EEG) recording

Animal surgery and video-EEG data collection was performed by the UTSW Neuro-Models Facility. Thirty-two adult mice at 11 mo of age were used in the EEG experiments with 8 in each experimental group (WT, RyanR3$^{-/-}$, APPPS1, and APPPS1xRyanR3$^{-/-}$). Mice were anesthetized using a gas anesthesia machine with ~1–2% isoflurane in a 1 L/min mixture of 70% nitrous oxide and 30% oxygen. Four epidural recording electrodes made from #00–90 x 1/8 inch stainless steel screws were placed at the following stereotaxic coordinates from bregma: A-P +1.0 mm, lateral ± 1.5 mm and A-P - 3.0 mm, lateral ± 1.5 mm along with a reference and ground screw over the olfactory bulb and cerebellum respectively. Electrodes were attached by a flexible wire (KYNAR, 30 ga) to a custom 6-pin micro-connector (Omnetics Connector Corporation) and secured with dental acrylic. Mice received the analgesic buprenorphine (0.05 mg/kg, Sigma, B9275) as necessary following surgery and were allowed to recover for at least 7 d prior to any experimentation. Following recovery from electrode implantation, each mouse was placed in a custom acrylic recording cage (Marsh Designs) and connected to a Tucker-Davis Technologies RZ2/PZ3 neurophysiology workstation through a flexible cable suspended from the top of the cage with an interposed commutator to allow mice free access to food

and water without twisting the cable. Continuous video/EEG (300 Hz sampling) was recorded for each mouse simultaneously for 7 d and read by a user blinded to the experimental grouping for the presence of seizures and epileptiform activity. Seizure activity was marked at the beginning and end of each event to account for seizure duration, and the numbers of seizures for each mouse was noted.

Statistical analysis

The results are presented as mean ± SE and comparisons of means were performed by 1-way ANOVA or Student *t* test. Means were considered to be significantly different when the p-value was < 0.05 and are indicated in text and figure legends.

Disclosure of Potential Conflicts of Interest

No potential conflicts of interest were disclosed.

Acknowledgments

We would like to thank Xia Liang for her help with genotyping of APPPS1, APPPS1xRyanR3$^{-/-}$ and RyanR3$^{-/-}$ mice and Leah Taylor for administrative assistance. EEG surgery and data collection was performed by the UTSW Neuro-Models Facility supported by the Haggerty Center for Brain Injury and Repair. IB is a holder of the Carl J and Hortense M Thomsen Chair in Alzheimer Disease Research. This work was supported by the Dynasty Foundation grant DP–B-11/13 (EP), Welch Foundation grant I-1754 (IB), NIH grant R01NS080152 (IB), and by the contract with the Russian Ministry of Science 11.G34.31.0056 (IB).

Supplemental Material

Supplemental material may be found here: http://www.landesbioscience.com/journals/channels/article/27471/

References

1. Bezprozvanny I, Mattson MP. Neuronal calcium mishandling and the pathogenesis of Alzheimer's disease. Trends Neurosci 2008; 31:454-63; PMID:18675468; http://dx.doi.org/10.1016/j.tins.2008.06.005
2. Bezprozvanny I. Calcium signaling and neurodegenerative diseases. Trends Mol Med 2009; 15:89-100; PMID:19230774; http://dx.doi.org/10.1016/j.molmed.2009.01.001
3. Supnet C, Bezprozvanny I. Neuronal calcium signaling, mitochondrial dysfunction, and Alzheimer's disease. J Alzheimers Dis 2010; 20(Suppl 2):S487-98; PMID:20413848
4. Supnet C, Bezprozvanny I. The dysregulation of intracellular calcium in Alzheimer disease. Cell Calcium 2010; 47:183-9; PMID:20080301; http://dx.doi.org/10.1016/j.ceca.2009.12.014
5. Popugaeva E, Supnet C, Bezprozvanny I. Presenilins, deranged calcium homeostasis, synaptic loss and dysfunction in Alzheimer's disease. Messenger 2012; 1:53-62; http://dx.doi.org/10.1166/msr.2012.1002
6. Bezprozvanny I, Hiesinger PR. The synaptic maintenance problem: membrane recycling, Ca2+ homeostasis and late onset degeneration. Mol Neurodegener 2013; 8:23; PMID:23829673; http://dx.doi.org/10.1186/1750-1326-8-23
7. Ito E, Oka K, Etcheberrigaray R, Nelson TJ, McPhie DL, Tofel-Grehl B, Gibson GE, Alkon DL. Internal Ca2+ mobilization is altered in fibroblasts from patients with Alzheimer disease. Proc Natl Acad Sci U S A 1994; 91:534-8; PMID:8290560; http://dx.doi.org/10.1073/pnas.91.2.534
8. Stutzmann GE, Smith I, Caccamo A, Oddo S, Laferla FM, Parker I. Enhanced ryanodine receptor recruitment contributes to Ca2+ disruptions in young, adult, and aged Alzheimer's disease mice. J Neurosci 2006; 26:5180-9; PMID:16687509; http://dx.doi.org/10.1523/JNEUROSCI.0739-06.2006
9. Kelliher M, Fastbom J, Cowburn RF, Bonkale W, Ohm TG, Ravid R, Sorrentino V, O'Neill C. Alterations in the ryanodine receptor calcium release channel correlate with Alzheimer's disease neurofibrillary and beta-amyloid pathologies. Neuroscience 1999; 92:499-513; PMID:10408600; http://dx.doi.org/10.1016/S0306-4522(99)00042-1
10. Bruno AM, Huang JY, Bennett DA, Marr RA, Hastings ML, Stutzmann GE. Altered ryanodine receptor expression in mild cognitive impairment and Alzheimer's disease. Neurobiol Aging 2012; 33:1001 e1-6.
11. Chan SL, Mayne M, Holden CP, Geiger JD, Mattson MP. Presenilin-1 mutations increase levels of ryanodine receptors and calcium release in PC12 cells and cortical neurons. J Biol Chem 2000; 275:18195-200; PMID:10764737; http://dx.doi.org/10.1074/jbc.M000040200
12. Zhang H, Sun S, Herreman A, De Strooper B, Bezprozvanny I. Role of presenilins in neuronal calcium homeostasis. J Neurosci 2010; 30:8566-80; PMID:20573903; http://dx.doi.org/10.1523/JNEUROSCI.1554-10.2010
13. Supnet C, Grant J, Kong H, Westaway D, Mayne M. Amyloid-beta-(1-42) increases ryanodine receptor-3 expression and function in neurons of TgCRND8 mice. J Biol Chem 2006; 281:38440-7; PMID:17050533; http://dx.doi.org/10.1074/jbc.M606736200
14. van de Vrede Y, Fossier P, Baux G, Joels M, Chameau P. Control of IsAHP in mouse hippocampus CA1 pyramidal neurons by RyR3-mediated calcium-induced calcium release. Pflugers Arch 2007; 455:297-308; PMID:17562071; http://dx.doi.org/10.1007/s00424-007-0277-4
15. Sah P, Faber ES. Channels underlying neuronal calcium-activated potassium currents. Prog Neurobiol 2002; 66:345-53; PMID:12015199; http://dx.doi.org/10.1016/S0301-0082(02)00004-7
16. Reyes M, Stanton PK. Induction of hippocampal long-term depression requires release of Ca2+ from separate presynaptic and postsynaptic intracellular stores. J Neurosci 1996; 16:5951-60; PMID:8815877
17. Futatsugi A, Kato K, Ogura H, Li ST, Nagata E, Kuwajima G, Tanaka K, Itohara S, Mikoshiba K. Facilitation of NMDAR-independent LTP and spatial learning in mutant mice lacking ryanodine receptor type 3. Neuron 1999; 24:701-13; PMID:10595520; http://dx.doi.org/10.1016/S0896-6273(00)81123-X
18. Galeotti N, Quattrone A, Vivoli E, Norcini M, Bartolini A, Ghelardini C. Different involvement of type 1, 2, and 3 ryanodine receptors in memory processes. Learn Mem 2008; 15:315-23; PMID:18441289; http://dx.doi.org/10.1101/lm.929008
19. Supnet C, Noonan C, Richard K, Bradley J, Mayne M. Up-regulation of the type 3 ryanodine receptor is neuroprotective in the TgCRND8 mouse model of Alzheimer's disease. J Neurochem 2010; 112:356-65; PMID:19903243; http://dx.doi.org/10.1111/j.1471-4159.2009.06487.x
20. Oulès B, Del Prete D, Greco B, Zhang X, Lauritzen I, Sevalle J, Moreno S, Paterlini-Bréchot P, Trebak M, Checler F, et al. Ryanodine receptor blockade reduces amyloid-β load and memory impairments in Tg2576 mouse model of Alzheimer disease. J Neurosci 2012; 32:11820-34; PMID:22915123; http://dx.doi.org/10.1523/JNEUROSCI.0875-12.2012
21. Peng J, Liang G, Inan S, Wu Z, Joseph DJ, Meng Q, Peng Y, Eckenhoff MF, Wei H. Dantrolene ameliorates cognitive decline and neuropathology in Alzheimer triple transgenic mice. Neurosci Lett 2012; 516:274-9; PMID:22516463; http://dx.doi.org/10.1016/j.neulet.2012.04.008
22. Chakroborty S, Briggs C, Miller MB, Goussakov I, Schneider C, Kim J, Wicks J, Richardson JC, Conklin V, Cameransi BG, et al. Stabilizing ER Ca2+ channel function as an early preventative strategy for Alzheimer's disease. PLoS One 2012; 7:e52056; PMID:23284867; http://dx.doi.org/10.1371/journal.pone.0052056
23. Zhao X, Weisleder N, Han X, Pan Z, Parness J, Brotto M, Ma J. Azumolene inhibits a component of store-operated calcium entry coupled to the skeletal muscle ryanodine receptor. J Biol Chem 2006; 281:33477-86; PMID:16945924; http://dx.doi.org/10.1074/jbc.M602306200
24. Giannini G, Conti A, Mammarella S, Scrobogna M, Sorrentino V. The ryanodine receptor/calcium channel genes are widely and differentially expressed in murine brain and peripheral tissues. J Cell Biol 1995; 128:893-904; PMID:7876312; http://dx.doi.org/10.1083/jcb.128.5.893
25. Krause T, Gerbershagen MU, Fiege M, Weisshorn R, Wappler F. Dantrolene--a review of its pharmacology, therapeutic use and new developments. Anaesthesia 2004; 59:364-73; PMID:15023108; http://dx.doi.org/10.1111/j.1365-2044.2004.03658.x
26. Bertocchini F, Ovitt CE, Conti A, Barone V, Schöler HR, Bottinelli R, Reggiani C, Sorrentino V. Requirement for the ryanodine receptor type 3 for efficient contraction in neonatal skeletal muscles. EMBO J 1997; 16:6956-63; PMID:9384575; http://dx.doi.org/10.1093/emboj/16.23.6956
27. Radde R, Bolmont T, Kaeser SA, Coomaraswamy J, Lindau D, Stoltze L, Calhoun ME, Jäggi F, Wolburg H, Gengler S, et al. Abeta42-driven cerebral amyloidosis in transgenic mice reveals early and robust pathology. EMBO Rep 2006; 7:940-6; PMID:16906128; http://dx.doi.org/10.1038/sj.embor.7400784
28. Takeshima H, Komazaki S, Hirose K, Nishi M, Noda T, Iino M. Embryonic lethality and abnormal cardiac myocytes in mice lacking ryanodine receptor type 2. EMBO J 1998; 17:3309-16; PMID:9628868; http://dx.doi.org/10.1093/emboj/17.12.3309

29. Lanner JT, Georgiou DK, Joshi AD, Hamilton SL. Ryanodine receptors: structure, expression, molecular details, and function in calcium release. Cold Spring Harb Perspect Biol 2010; 2:a003996; PMID:20961976; http://dx.doi.org/10.1101/cshperspect.a003996
30. Tang TS, Guo C, Wang H, Chen X, Bezprozvanny I. Neuroprotective effects of inositol 1,4,5-trisphosphate receptor C-terminal fragment in a Huntington's disease mouse model. J Neurosci 2009; 29:1257-66; PMID:19193873; http://dx.doi.org/10.1523/JNEUROSCI.4411-08.2009
31. Kasumu AW, Liang X, Egorova P, Vorontsova D, Bezprozvanny I. Chronic suppression of inositol 1,4,5-triphosphate receptor-mediated calcium signaling in cerebellar purkinje cells alleviates pathological phenotype in spinocerebellar ataxia 2 mice. J Neurosci 2012; 32:12786-96; PMID:22973002; http://dx.doi.org/10.1523/JNEUROSCI.1643-12.2012
32. Balschun D, Wolfer DP, Bertocchini F, Barone V, Conti A, Zuschratter W, Missiaen L, Lipp HP, Frey JU, Sorrentino V. Deletion of the ryanodine receptor type 3 (RyR3) impairs forms of synaptic plasticity and spatial learning. EMBO J 1999; 18:5264-73; PMID:10508160; http://dx.doi.org/10.1093/emboj/18.19.5264
33. Palop JJ, Chin J, Roberson ED, Wang J, Thwin MT, Bien-Ly N, Yoo J, Ho KO, Yu GQ, Kreitzer A, et al. Aberrant excitatory neuronal activity and compensatory remodeling of inhibitory hippocampal circuits in mouse models of Alzheimer's disease. Neuron 2007; 55:697-711; PMID:17785178; http://dx.doi.org/10.1016/j.neuron.2007.07.025
34. Hardy J, Selkoe DJ. The amyloid hypothesis of Alzheimer's disease: progress and problems on the road to therapeutics. Science 2002; 297:353-6; PMID:12130773; http://dx.doi.org/10.1126/science.1072994
35. Hyman BT. Amyloid-dependent and amyloid-independent stages of Alzheimer disease. Arch Neurol 2011; 68:1062-4; PMID:21482918; http://dx.doi.org/10.1001/archneurol.2011.70
36. Kasai H, Matsuzaki M, Noguchi J, Yasumatsu N, Nakahara H. Structure-stability-function relationships of dendritic spines. Trends Neurosci 2003; 26:360-8; PMID:12850432; http://dx.doi.org/10.1016/S0166-2236(03)00162-0
37. Bourne JN, Harris KM. Balancing structure and function at hippocampal dendritic spines. Annu Rev Neurosci 2008; 31:47-67; PMID:18284372; http://dx.doi.org/10.1146/annurev.neuro.31.060407.125646
38. Bourne J, Harris KM. Do thin spines learn to be mushroom spines that remember? Curr Opin Neurobiol 2007; 17:381-6; PMID:17498943; http://dx.doi.org/10.1016/j.conb.2007.04.009
39. Penzes P, Cahill ME, Jones KA, VanLeeuwen JE, Woolfrey KM. Dendritic spine pathology in neuropsychiatric disorders. Nat Neurosci 2011; 14:285-93; PMID:21346746; http://dx.doi.org/10.1038/nn.2741
40. Dickstein DL, Weaver CM, Luebke JI, Hof PR. Dendritic spine changes associated with normal aging. Neuroscience 2012; In press; PMID:23069756.
41. Luebke JI, Weaver CM, Rocher AB, Rodriguez A, Crimins JL, Dickstein DL, Wearne SL, Hof PR. Dendritic vulnerability in neurodegenerative disease: insights from analyses of cortical pyramidal neurons in transgenic mouse models. Brain Struct Funct 2010; 214:181-99; PMID:20177698; http://dx.doi.org/10.1007/s00429-010-0244-2
42. Tackenberg C, Ghori A, Brandt R. Thin, stubby or mushroom: spine pathology in Alzheimer's disease. Curr Alzheimer Res 2009; 6:261-8; PMID:19519307; http://dx.doi.org/10.2174/156720509788486554
43. Tackenberg C, Brandt R. Divergent pathways mediate spine alterations and cell death induced by amyloid-beta, wild-type tau, and R406W tau. J Neurosci 2009; 29:14439-50; PMID:19923278; http://dx.doi.org/10.1523/JNEUROSCI.3590-09.2009
44. Dumitriu D, Rodriguez A, Morrison JH. High-throughput, detailed, cell-specific neuroanatomy of dendritic spines using microinjection and confocal microscopy. Nat Protoc 2011; 6:1391-411; PMID:21886104; http://dx.doi.org/10.1038/nprot.2011.389
45. Rodriguez A, Ehlenberger DB, Dickstein DL, Hof PR, Wearne SL. Automated three-dimensional detection and shape classification of dendritic spines from fluorescence microscopy images. PLoS One 2008; 3:e1997.
46. Wegenast-Braun BM, Fulgencio Maisch A, Eicke D, Radde R, Herzig MC, Staufenbiel M, Jucker M, Calhoun ME. Independent effects of intra- and extracellular Abeta on learning-related gene expression. Am J Pathol 2009; 175:271-82; PMID:19556514; http://dx.doi.org/10.2353/ajpath.2009.090044
47. Kamenetz F, Tomita T, Hsieh H, Seabrook G, Borchelt D, Iwatsubo T, Sisodia S, Malinow R. APP processing and synaptic function. Neuron 2003; 37:925-37; PMID:12670422; http://dx.doi.org/10.1016/S0896-6273(03)00124-7
48. Cirrito JR, Yamada KA, Finn MB, Sloviter RS, Bales KR, May PC, Schoepp DD, Paul SM, Mennerick S, Holtzman DM. Synaptic activity regulates interstitial fluid amyloid-beta levels in vivo. Neuron 2005; 48:913-22; PMID:16364896; http://dx.doi.org/10.1016/j.neuron.2005.10.028
49. van Gelder BM, Buijsse B, Tijhuis M, Kalmijn S, Giampaoli S, Nissinen A, Kromhout D. Coffee consumption is inversely associated with cognitive decline in elderly European men: the FINE Study. Eur J Clin Nutr 2007; 61:226-32; PMID:16929246; http://dx.doi.org/10.1038/sj.ejcn.1602495
50. Ritchie K, Carrière I, de Mendonca A, Portet F, Dartigues JF, Rouaud O, Barberger-Gateau P, Ancelin ML. The neuroprotective effects of caffeine: a prospective population study (the Three City Study). Neurology 2007; 69:536-45; PMID:17679672; http://dx.doi.org/10.1212/01.wnl.0000266670.35219.0c
51. Eskelinen MH, Ngandu T, Tuomilehto J, Soininen H, Kivipelto M. Midlife coffee and tea drinking and the risk of late-life dementia: a population-based CAIDE study. J Alzheimers Dis 2009; 16:85-91; PMID:19158424
52. Laitala VS, Kaprio J, Koskenvuo M, Räihä I, Rinne JO, Silventoinen K. Coffee drinking in middle age is not associated with cognitive performance in old age. Am J Clin Nutr 2009; 90:640-6; PMID:19587088; http://dx.doi.org/10.3945/ajcn.2009.27660
53. Cao C, Loewenstein DA, Lin X, Zhang C, Wang L, Duara R, Wu Y, Giannini A, Bai G, Cai J, et al. High Blood caffeine levels in MCI linked to lack of progression to dementia. J Alzheimers Dis 2012; 30:559-72; PMID:22430531
54. Cao C, Cirrito JR, Lin X, Wang L, Verges DK, Dickson A, Mamcarz M, Zhang C, Mori T, Arendash GW, et al. Caffeine suppresses amyloid-beta levels in plasma and brain of Alzheimer's disease transgenic mice. J Alzheimers Dis 2009; 17:681-97; PMID:19581723
55. Arendash GW, Schleif W, Rezai-Zadeh K, Jackson EK, Zacharia LC, Cracchiolo JR, Shippy D, Tan J. Caffeine protects Alzheimer's mice against cognitive impairment and reduces brain beta-amyloid production. Neuroscience 2006; 142:941-52; PMID:16938404; http://dx.doi.org/10.1016/j.neuroscience.2006.07.021
56. Arendash GW, Mori T, Cao C, Mamcarz M, Runfeldt M, Dickson A, Rezai-Zadeh K, Tane J, Citron BA, Lin X, et al. Caffeine reverses cognitive impairment and decreases brain amyloid-beta levels in aged Alzheimer's disease mice. J Alzheimers Dis 2009; 17:661-80; PMID:19581722
57. Qosa H, Abuznait AH, Hill RA, Kaddoumi A. Enhanced brain amyloid-β clearance by rifampicin and caffeine as a possible protective mechanism against Alzheimer's disease. J Alzheimers Dis 2012; 31:151-65; PMID:22504320
58. Espinosa J, Rocha A, Nunes F, Costa MS, Schein V, Kazlauckas V, Kalinine E, Souza DO, Cunha RA, Porciúncula LO. Caffeine consumption prevents memory impairment, neuronal damage, and adenosine A2A receptors upregulation in the hippocampus of a rat model of sporadic dementia. J Alzheimers Dis 2013; 34:509-18; PMID:23241554
59. Shimizu H, Fukaya M, Yamasaki M, Watanabe M, Manabe T, Kamiya H. Use-dependent amplification of presynaptic Ca2+ signaling by axonal ryanodine receptors at the hippocampal mossy fiber synapse. Proc Natl Acad Sci U S A 2008; 105:11998-2003; PMID:18687898; http://dx.doi.org/10.1073/pnas.0802175105